

A high-rate foreground of sub-second flares from geosynchronous satellites

Guy Nir,^{*} Eran O. Ofek, Sagi Ben-Ami, Noam Segev, David Polishook, Ilan Manulis

Department of Particle Physics and Astrophysics, Weizmann Institute of Science, 76100 Rehovot, Israel

Accepted XXX. Received YYY; in original form ZZZ

ABSTRACT

The Weizmann Fast Astronomical Survey Telescope (W-FAST) is a 55 cm optical survey telescope with a high cadence (25 Hz) monitoring of the sky over a wide field of view (7 deg^2). The high frame rate allows detection of sub-second transients over multiple images. We present a sample of $\sim 0.1\text{--}0.3 \text{ s}$ duration flares detected in an un-targeted survey for such transients. We show that most, if not all of them, are glints of sunlight reflected off geosynchronous and graveyard orbit satellites. The flares we detect have a typical magnitude of 9–11, which translates to $\sim 14\text{--}16$ th magnitude if diluted by a 30 s exposure time. We estimate the rate of events brighter than $\sim 11 \text{ mag}$ to be on the order of 30–40 events per day per deg^2 , for declinations between -20 and $+10^\circ$, not including the declination corresponding to the geostationary belt directly above the equator, where the rate can be higher. We propose that such glints are common in large area surveys (e.g., ZTF and LSST), and that some of them would have a point-like appearance, confounding searches for fast transients such as Fast Radio Burst counterparts. By observing in the direction of the Earth’s shadow we are able to put an upper limit on the rate of fast astrophysical transients of $0.052 \text{ deg}^{-2} \text{ day}^{-1}$ (95% confidence limit) for events brighter than 11 mag.

Key words: surveys – transients – techniques: photometric

1 INTRODUCTION

There are few known astronomical transients with durations lasting less than a second. Some examples include Gamma Ray Bursts (GRBs; Waxman & Bahcall 1997) and Fast Radio Bursts (FRBs; Lorimer et al. 2007). Stellar objects typically produce flares on time-scales of seconds to tens of minutes (Balona 2015; West et al. 2015). Optical phenomena on sub-second time-scales may include, e.g., FRB counterparts or collisions or outbursts of small objects in the Solar System. Since only a few optical telescopes observe a large field of view, and also take data at a cadence higher than once-per-second, the lack of detections of such transients is perhaps not surprising. Some notable examples for such surveys include mostly occultation surveys using small telescopes (Zhang et al. 2013; Wang et al. 2016; Arimatsu et al. 2017; Pass et al. 2018) but also larger telescopes with deeper limiting magnitude, although at a more modest field of view and cadence (Sako et al. 2018). These surveys are mostly focused on dips in the lightcurves of bright stars, and not on blind searches for sub-second transients. Some efforts have been made to explore this specific parameter space, but no outstanding discoveries have been made to date (e.g., Andreoni et al. 2020a,b; Chen et al. 2020; De et al. 2020).

Large area surveys that are running blind searches for transients on a large field of view can detect such sources, but they would be diluted by the long exposure time of the survey, with typical exposure times of 15–60 s, e.g., the Legacy Survey of Space and Time (LSST; Ivezić 2007) or the Zwicky Transient Facility (ZTF; Bellm et al. 2019). Even if the flare is bright enough to be seen when diluted by a factor of 10–100, it will still be hard to differentiate the flare from

other artefacts, primarily cosmic rays. If the system Point Spread Function (PSF) is well sampled, the shape of typical cosmic ray hits will usually be very different from an astronomical source, but when the image scale is similar to the PSF size, cosmic rays that deposit their energy in a small cluster of pixels will be hard to discern from optical sources. For this reason, many surveys ignore transients that appear in single images.

The Weizmann Fast Astronomical Survey Telescope (W-FAST; Nir et al. 2017, 2020) system was designed specifically to explore the parameter space of large field of view and high cadence. The W-FAST main survey takes images with a field of view of 7 deg^2 and a cadence of 25 Hz. This makes it well suited for finding transients lasting between 0.04 and 1 s, and brighter than 13 mag.

We present detections of flares with typical duration of 0.2s and brightness of 9–11 mag. While some flares’ origins remain uncertain, most flares can be definitively associated with short glints from geosynchronous satellites. Since the duration and brightness of all the events in our datasets are similar, we argue that all such flares are likely satellite glints. It has long been known that satellite glints (as well as meteors) can produce flashes in naked eye observations and photometer readings (Schaefer et al. 1987a,b). In this case, however, the flashes are caused by high-orbit satellites, that can appear to be motionless even in arcsecond-resolution images. Recently, Corbett et al. (2020) presented a sample of short time-scale glints. The sample in that work is larger than that presented here, allowing them to better characterize the magnitude distribution of flares at different regions of the sky. We find a rate that is an order of magnitude larger than the rate they find for satellites in the equatorial region. One possible explanation for this discrepancy is W-FAST system’s higher cadence, which allows us to detect fainter objects. Since the flare duration is usually longer than the W-FAST exposure time, their light is

^{*} E-mail: guy.nir@weizmann.ac.il

not diluted, and we can measure their peak magnitude independently of the glint duration. In addition, the W-FAST system's smaller pixel scale allows us to differentiate between low-orbit satellites that are clearly streaked and high-orbit satellites that can be mistaken for point sources. [Blake et al. \(2020\)](#) have studied satellites, spent rockets and smaller debris at geosynchronous altitude, showing the existence of a population of objects with typical sizes of tens of cm or smaller, that are often tumbling or rotating. These objects are good candidates for creating the glints we present in this work.

We argue that sub-second time-scale glints, particularly those of high orbit satellites, are a common foreground to synoptic surveys. These glints should be considered when discussing survey strategies such as splitting a single integration into several exposures.

In Section 2 we present the data acquisition and the observational sample, in Section 3 we present the results of our analysis of a set of flares and their properties, in Section 4 we explain the nature of point-source flares in our data, and in Section 5 we discuss the results and the implications for fast transients searches.

2 OBSERVATIONS

We used the W-FAST system, which spends most of its time taking high cadence (25 Hz) images of dense fields. The system has a pixel scale of $2.29'' \text{ pix}^{-1}$ and is described by Nir et al (in prep). Observations reported in this work were obtained using the F505W filter (rectangular band pass between 400 to 610 nm). During these observations, the full-frame images are not saved, as the data rate of about 6 Gbits s^{-1} is too large to store continuously.¹ The camera produces batches of one hundred images every four seconds, and we produce cutouts and stack images from these full frame images, which are then discarded. The cutouts include 15×15 pixels around ≈ 2000 stars, and the stack images include the full sensor data, but on a cadence of 4 s.

In addition to cutouts around stars we also run a custom algorithm that, in real time, identifies local maxima in the entire image. To make the detection process fast enough to run in real time over the full-frame data set, we trigger on a single pixel surpassing 256 ADU. This excludes most noise sources (with typical per-pixel rms of ~ 3 ADU) and allows us to scan only the most significant byte out of the two bytes representing each pixel. The high threshold is not adjusted for observing conditions such as seeing, background or airmass, and the detection pipeline does not account for the light spread outside the brightest pixel. This makes for a very inefficient detection method, which is designed for speed rather than sensitivity. The threshold of 256 ADU corresponds to an average magnitude of ≈ 10 , depending on observing conditions.

When peaks are identified, a cutout around each peak is saved, including a 15×15 stamp around the peak location, for each of the one hundred frames in that batch. These cutouts are then checked for flares lasting more than one frame, and those are saved for further processing. The majority of peaks that are detected are cosmic rays, which hit the sensor at a rate of $\approx 0.5 \text{ s}^{-1}$. These appear in a single frame and thus are not saved. Since we began collecting flares in a systematic way we have detected a few each night.

We present a sample of the observations taken during 2020 August–September. There are a number of fields observed either on or off the ecliptic plane. We disqualify runs where data quality was poor, e.g.,

¹ The data rate is approximately twice that of the planned LSST, assuming it produces 3.2 Gigapixel, 16-bit images every 15 seconds, and twice of that of the Large Array Survey Telescope (Ofek & Ben-Ami, in prep).

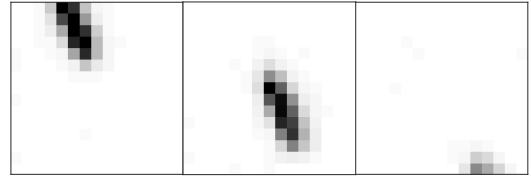


Figure 1. An example of a low Earth orbit satellite. The PSF of each individual image is clearly streaked, and the motion of the object between frames is apparent. The (inverted) scale for each image is the same, with the peak pixel value of 763 ADU in the first frame and 616 ADU in the central frame.

if the software crashed and did not save the flare data as expected. A summary of the observing runs is shown in Table 1.

3 RESULTS

Some of the flares detected by our system were clearly Low Earth Orbit (LEO) satellites. These move at hundreds of arcseconds per second and are visibly streaked even in the high-cadence data. An example for such a streak is shown in Figure 1.

We disqualify such streaks using hypothesis testing that is done by comparing the Signal to Noise ratio (S/N) calculated in two ways: (a) the S/N assuming the object is a point source, using a standard matched-filter ([Turin 1960](#)) with a gaussian kernel that has a width of $\sigma_g = 1$ pixel; (b) the S/N assuming the object is streaked, which we find using the the Radon transform map S_R of the above-mentioned, filtered image. The Radon transform sums the pixels along lines of different angle and starting position ([Radon 1917](#); [Parks 1986](#)). To normalize the sum of pixels to the noise from those pixels, we also calculate the Radon transform of a uniform map, V_R , representing the background variance, and divide the two maps to get

$$(S/N)_R = \frac{S_R}{\sqrt{V_R}}. \quad (1)$$

The maximum of $(S/N)_R$ represents the signal-to-noise ratio of a streaked object. This method has been shown to be optimal for detection of streaks in background dominated images ([Nir et al. 2018](#)). In both cases we first subtract the median of the cutout to try and reduce the background. To increase the S/N of short streaks, we first crop the image to the central 7 pixels around the brightest point, before using the Radon transform. A simple hypothesis test ([Neyman & Pearson 1933](#)) checks if the Radon S/N is higher than the point source S/N by a factor² larger than $\sqrt{2}$, and if so, we assume it is a streaked source and do not include it in the sample. Furthermore, we disqualify flares occurring less than 6 pixels from the edge of the sensor.

In Figure 2 we show the shape and temporal behavior of one set of such flares, detected within a few minutes of each other. Each row in the Figure is a separate flare, showing that each event brightens and fades in about 0.2 seconds. The shape of each image hotspot is consistent with the system PSF. The images were collected on 2020 August 6th, around 22:38:00 (UTC) within a field centered on right ascension of $22^h 04^m 01.3^s$ and declination of $-10^\circ 29' 54.7''$

² To accommodate the width of the PSF, which is equivalent to a short streak of width 1–2 pixels, we increase the threshold for identifying an object as a point source by a factor of $\sqrt{2}$, which is the expected increase for a two-pixel streak.

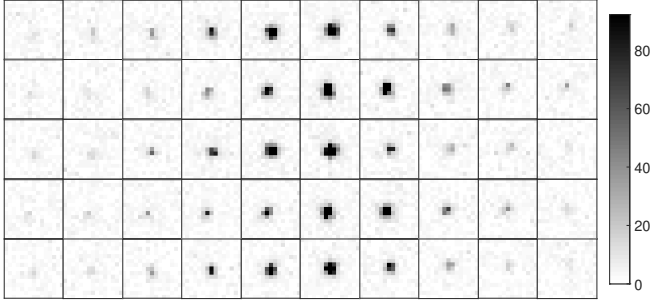


Figure 2. Examples for five glints taken at different locations in the same field of view, within the time span of a few minutes. Each row is for a separate flare, showing ten consecutive frames around the area of the peak. The images are all set to the same (inverted) scale, that shows the range of brightnesses as the flare appears and fades. The flares have a typical time-scale of 3–5 frames, or 0.12–0.2 s.

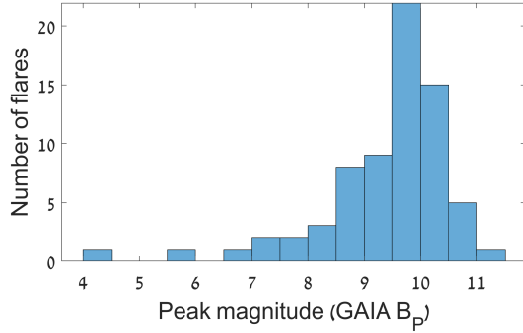


Figure 3. Peak magnitude of glints detected in this sample. The flux of each glint is compared, at peak, with the current image zero-point, based on the magnitudes and fluxes of other stars in the image. The stars' magnitude is matched to the GAIA DR2 B_P filter. For objects with multiple glints we plot the brightest magnitude. The scatter for multiple glints is typically less than one magnitude.

(J2000). Each flare appears to be stationary in the images, ruling out objects in LEO that appear streaked even in single frames.

We observed for 119.40 hours, found 1341 LEO satellites, and 862 point-source flares, which we associate with 76 distinct objects, as explained in the next Section, that discusses repeating flares.

For each flare we calculate the flux using an aperture of 3 pixels radius ($6.87''$) that is centred on the position of the flare. We subtract the background using an annulus with inner and outer radii of 7.5 and 10 pixels (17.2 and $23''$). The flux for each frame is compared to the image zero point calculated against other stars using the same photometric pipeline. The stars' magnitudes are compared to the GAIA B_P filter data from DR2 (Gaia Collaboration 2018), using tools developed by Ofek (2014) and Soumagnac & Ofek (2018), with astrometric solutions given by Ofek (2019). The flares commonly have a magnitude of 9–11 in this band. A histogram of the peak magnitude of all flares is shown in Figure 3. For repeating flares we include the maximum magnitude of all repeated flares (see discussion below). Repeated flares typically have a magnitude scatter less than 1 mag.

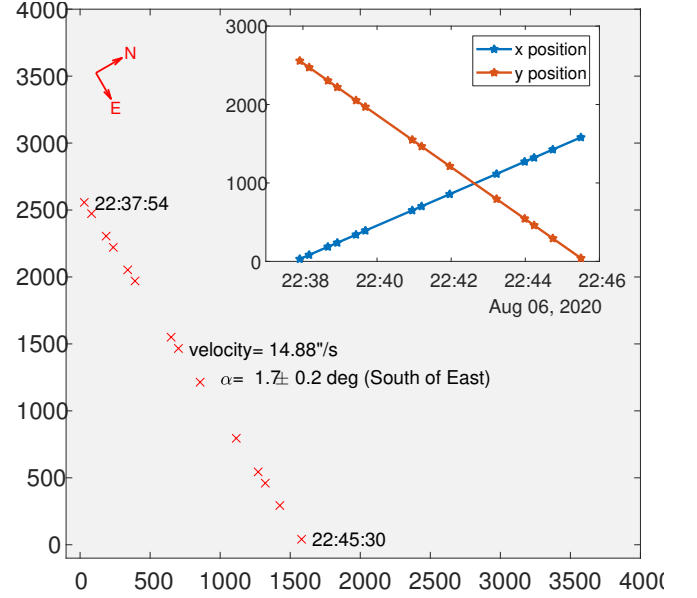


Figure 4. Position of repeating flares from the same object as shown in Figure 2. The larger plot shows the position of the object at each point on the sensor where a flare occurred. We associated 14 different flares with this object, all aligned in a straight line. The start and end points are marked with the UTC times of the first and last flare in this set. The inset shows the x and y position of the object as a function of time. The velocity of the object is measured to be close to $14.88''$ per second. The object's velocity's position angle is $91.7 \pm 0.2^\circ$ (Measured from North towards East). The time delay between flares is not constant. Clearly the flares are coming from a geosynchronous satellite.

4 THE NATURE OF THE FLARES

The example set of flares in Figure 2 shows five flares out of 14, detected in the same field of view, within the time frame of a few minutes. The flares do not repeat at the same location, moving hundreds of arcseconds during tens of seconds between flares, spread along a straight line. We thus assume these flares are associated with a single, repeating object. Of course the rate of motion disqualifies the object from being outside the Solar System. Measuring the position of the flares in time across the field of view, as shown in Figure 4, gives the velocity of the source to be $14.88 \text{ arcsec s}^{-1}$, at an angle of $\approx 2^\circ$ South of the East direction, consistent with what we expect from geosynchronous satellites. The majority of flares repeating in a single field can be grouped in this way into repeating objects moving with similar rates along a straight line. We therefore conclude that this repeating flare, and most likely all similar sources in our sample, are in fact glints from geosynchronous satellites.

In this specific example the time delay between flashes are 15.1589 30.4057 15.1977 30.3176 15.1588 75.8721 15.1980 45.5155 75.8325 45.5143 15.1991 30.3164 45.5151 s, repeating in multiples of 15.1589 s, where the multiplication is not in any particular pattern. The duration of each flare, taking 3–5 frames to appear and disappear, can be translated to the instantaneous angular velocity, if we model the flashes as coming from a flat, mirror-like surface:

$$\omega \approx \frac{D_{\text{ang,sun}}}{2N_{\text{frames}}\Delta T} = 1.56^{+0.52}_{-0.31} \text{ deg s}^{-1}, \quad (2)$$

where $D_{\text{ang,sun}}$ is the sun angular size, in degrees (0.5°), N_{frames} is the number of frames where the flash is seen, and ΔT is the time between frames. The angular frequency and its errors are calculated by setting

$N_{\text{frames}} = 4 \pm 1$. This translates to a period of $P = 230.4 \pm 57.6$ s. The fact that this period is longer than the typical time between flashes suggests there is more than one reflective surface, at different positions on the satellite. It is important to note that our sample includes several satellites with short intervals between flares, and others that show a single flare that does not repeat. The duration of flares is also not constant and lasts between one to seven frames.³ This suggests there are many rotation periods and many geometries for the reflecting surfaces on the satellites.

The mean magnitude of the peaks of the flares in the example discussed above is around 9.5 in GAIA B_P , likely due to the high detection threshold we used to discover them. If we model these flashes as reflections on a smooth, mirror-like, circular surface, we can estimate the size of the reflector based on the measured flux. The magnitude of the flash would be given by

$$M_{\text{ref}} = M_{\text{sun}} - 5 \log 10 \left(\frac{D_{\text{ang,ref}}}{D_{\text{ang,sun}}} \right) - 2.5 \log 10(A), \quad (3)$$

where $M_{\text{sun}} = -26.74$ is the Sun's apparent magnitude, A is the mirror albedo (fraction of flux reflected), and $D_{\text{ang,ref}}$ is the reflector angular diameter. We assume the satellite is on a circular orbit and was observed at an elevation angle of 47.9° , which gives a slant range of $R = 37,200$ km. Using this distance we can estimate the reflector's physical size:

$$D_{\text{ref}} = R_{\text{ref}} D_{\text{sun,ang}}^{(\text{radians})} 10^{(M_{\text{ref}} - M_{\text{sun}})/5} / \sqrt{A}. \quad (4)$$

For $M_{\text{ref}} = 9.7$ we get $D_{\text{ref}} = 1.8/\sqrt{A}$ in cm. If $A = 0.04$, typical of glass windows, we get a diameter of 9 cm.

In Figure 5, we plot the number of flaring objects as a function of the field declination. We do not count fields where the Earth's shadow intersects the line of sight to the coordinates of the field centre, at the orbital radius of geosynchronous satellites. In those fields, we did not detect any flares, but we do not include them in the rate calculations as satellites are not expected to be seen. To calculate the number of individual objects that often have multiple flares, we cluster the flares in each run according to the maximum velocity⁴ of $15'' \text{ s}^{-1}$. In Table 1 we specify for each run the number of individual objects and the average number of flares per object in that run, and whether that run is inside the Earth's shadow at the radius of geosynchronous satellites. The number of satellites and the number of hours per run, as a function of declination, is shown in Figure 5. The blue bars represent the number of hours observed in each 10° declination bin, while the red bars show the number of satellites detected. These include only satellites moving with a velocity consistent with geosynchronous orbit. The errors on the rate are 90% confidence intervals.

We see more satellites on low declinations (-20 to $+10^\circ$), which is reasonable as many geosynchronous satellites spend much of their time close to the equatorial plane. A very rough estimate of the lower limit on the rate of such glinting objects can be calculated from the number of observed objects and the observing time. We find

³ Most flares that appear in a single frame are excluded by our detection algorithm. Some flares are detected even though they show up in a single frame, if multiple single-frame flares, separated by a short interval, appear in the same 100 frame (4 second) batch.

⁴ The clustering was based solely on the distance and time between flares being consistent objects moving up to the velocity of $15'' \text{ s}^{-1}$. We did not require the flares to be on a straight line or to have similar magnitudes. Since glinting objects rarely appear at the same time and nearby on the sky, it is unlikely that flares would be associated with the wrong object during the clustering.

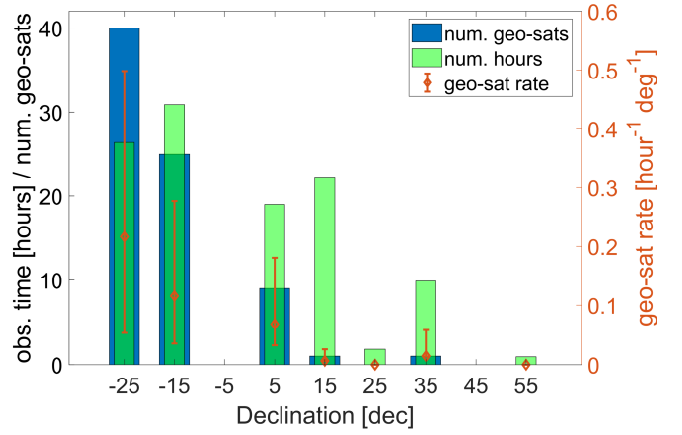


Figure 5. The number of hours and the number of geosynchronous satellites as a function of declination. Each satellite is comprised of one or multiple flares that were grouped based on velocity that is consistent with geosynchronous orbit.

the rate of individual flares, brighter than ~ 11 mag to be $1.73^{+0.17}_{-0.16} \text{ deg}^{-2} \text{ hour}^{-1}$ at a declination -25° , and a somewhat lower rate of $1.26^{+0.17}_{-0.16} \text{ deg}^{-2} \text{ hour}^{-1}$ at a declination of $+5^\circ$. The uncertainties account for 90% confidence on the Poisson distribution, but do not account for systematics as discussed below. If we count individual objects regardless of the number of repeat flares it displays, the rate is decreased by an order of magnitude, giving a rate of $0.22^{+0.07}_{-0.05} \text{ deg}^{-2} \text{ hour}^{-1}$ at declination -25° and $0.07^{+0.05}_{-0.03} \text{ deg}^{-2} \text{ hour}^{-1}$ at $+5^\circ$. These rates do not include geostationary satellites that are always on the equatorial plane.

From our observatory at latitude 30.59°N , the geostationary orbit is seen at an apparent declination of -5° . Unfortunately, we did not observe any fields in this declination, we cannot constrain the rate on the geostationary belt directly above the equator.

This small survey is not complete when it comes to counting satellites: the threshold for detection of strong peaks is constant, and set to a pixel value of 256 ADU, without considering changes in seeing, background, or airmass. The detection algorithm requires at least two frames to be five times brighter than the background, which excludes most flares lasting a single frame. Furthermore, some of the flares may have been counted as streaked if the seeing was particularly bad. Finally, the survey does not sample a wide range of coordinates on the sky in a systematic way, instead the survey strategy was determined by other considerations for other science goals.

During these observations, we have taken images of fields inside Earth's shadow (at the radius of geosynchronous satellites) for a total of 8.2 hours. In this direction no flares were detected, which gives an upper limit on the rate of astrophysical flares brighter than 11th magnitude of $0.052 \text{ deg}^{-2} \text{ hour}^{-1}$ (95% one-sided confidence limit).

5 CONCLUSIONS

Since we have begun a blind search for fast transients in the W-FAST data, we detected multiple instances of short duration flashes lasting ~ 0.2 s and reaching a typical brightness of 10-th magnitude. While we cannot rule out that some of these flashes come from stellar flares of astrophysical origin, we conclude that most or all of these events are satellite glints.

The size of the reflector required to produce such flares is cm-scale, if the object is purely reflective. If instead of a mirror we assume some transparent material like glass covering optics or solar panels, the size of the reflector would be on the 10 cm scale.

In our sample we have many examples where multiple flashes were seen from the same object. In most cases the time delays between flashes are non-uniform, and are much shorter than the rotation period we estimate based on the length of the flashes themselves. This suggests such satellites have several reflective surfaces of similar size and different orientations.

The threshold we used to blindly detect such short flares in our data is very high compared to the noise, suggesting that there are many other fainter, undetected glints. For individual flares the rate is $1.73^{+0.17}_{-0.16}$ and $1.26^{+0.17}_{-0.16}$ $\text{deg}^{-2} \text{hour}^{-1}$ at declination -25° and $+5^\circ$, respectively. For individual objects, counting all repeat flares into single objects, we find a rate of $0.22^{+0.07}_{-0.05}$ and $0.07^{+0.05}_{-0.03}$ $\text{deg}^{-2} \text{hour}^{-1}$ for declinations -25° and $+5^\circ$, respectively. This rate is an order of magnitude larger than the rate of glints reported by Corbett et al. (2020) for the equatorial region. One explanation for this difference is due to the fainter limiting magnitude of W-FAST. Our exposure time is shorter than the typical flare duration, so the flares' flux is not diluted by the exposure time. This allows us to observe fainter peak magnitudes, and indeed we see many more flares in the range 9–11 mag than flares brighter than 9 mag (see Figure 3).

Perhaps the most important conclusion is that these flashes are quite common and could look similar to a real astronomical source in other surveys that search for short duration transients. While satellites usually appear clearly streaked in long exposures (e.g., more than 1 second), the satellite's diffuse reflection may be too dim to detect, and only the short-duration flash would be seen. If the object rotates quickly, the duration of the flash may become shorter than 0.1 s, and the streaked nature of the flash, with a length of $< 1.5''$, would not be discernible under typical seeing conditions. So such a glint could have a similar shape as that of point sources in the image. For a survey like ZTF, with an exposure time of 30 s, the flashes could be diluted by a factor of more than 100, giving an effective magnitude of 15 or dimmer. These flashes would appear in a single image and would be very hard to discern from astrophysical sources.

While this survey hints that the rate of fast glints from geosynchronous satellites increases at low declination this cannot be taken as a rule. Satellites have a wide variety of orbits, and should always be considered as a foreground to fast transient searches.

Finding real astrophysical short-duration transients requires developing ways to deal with this very high rate of foreground events. One way to overcome this problem, in an un-targeted search for astrophysical fast transients, would be to scan only the area of the sky inside Earth's shadow. For geosynchronous satellites this patch has a radius of $\approx 10^\circ$, and it becomes smaller for satellites on even higher orbits, which are relatively few. Another possibility is to view the same field using two telescopes placed $\gtrsim 1$ km apart, so the parallax of flares can be measured. From our observations inside the Earth's shadow we can put an upper limit on flares brighter than 11th magnitude of $0.052 \text{ deg}^{-2} \text{hour}^{-1}$ (95% confidence level).

DATA AVAILABILITY

The data underlying this article will be shared on reasonable request to the corresponding author.

REFERENCES

- Andreoni I., et al., 2020a, *MNRAS*, **491**, 5852
 Andreoni I., et al., 2020b, *ApJ*, **896**, L2
 Arimatsu K., et al., 2017, *PASJ*, **69**, 68
 Balona L. A., 2015, *MNRAS*, **447**, 2714
 Bellm E. C., et al., 2019, *PASP*, **131**, 018002
 Blake J. A., et al., 2020, arXiv e-prints, p. arXiv:2008.12799
 Chen G., Ravi V., Lu W., 2020, *ApJ*, **897**, 146
 Corbett H., et al., 2020, arXiv e-prints, p. arXiv:2011.02495
 De K., et al., 2020, *ApJ*, **901**, L7
 Gaia Collaboration 2018, *A&A*, **616**, A1
 Ivezić Z., 2007, in American Astronomical Society Meeting Abstracts #210. p. 174
 Lorimer D. R., Bailes M., McLaughlin M. A., Narkevic D. J., Crawford F., 2007, *Science*, **318**, 777
 Neyman Pearson 1933, *Philosophical Transactions of the Royal Society of London A: Mathematical, Physical and Engineering Sciences*, **231**, 289
 Nir G., Ofek E. O., Ben-Ami S., Manulis I., Gal-Yam A., Diner O., Rappaport M., 2017, in American Astronomical Society Meeting Abstracts #229. p. 155.06
 Nir G., Zackay B., Ofek E. O., 2018, *AJ*, **156**, 229
 Nir G., Ofek E. O., Ben-Ami S., Noam S., Polishook D., Manulis I., Ofir H., 2020
 Ofek E. O., 2014, MATLAB package for astronomy and astrophysics, Astrophysics Source Code Library (ascl:1407.005)
 Ofek E. O., 2019, *PASP*, **131**, 054504
 Parks P. C., 1986, *IEEE Transactions on Medical Imaging*, **5**, 170
 Pass E., Metchev S., Brown P., Beauchemin S., 2018, *Publications of the Astronomical Society of the Pacific*, **130**, 014502
 Radon J., 1917, *Berichte über die Verhandlungen der Königlich-Sächsischen Akademie der Wissenschaften zu Leipzig, Mathematisch-Physische Klasse*, pp 262–277
 Sako S., et al., 2018, in *Proc. SPIE*, p. 107020J, doi:10.1117/12.2310049
 Schaefer B. E., Pedersen H., Gouiffes C., Poulsen J. M., Pizzichini G., 1987a, *A&A*, **174**, 338
 Schaefer B. E., et al., 1987b, *ApJ*, **320**, 398
 Soumagnac M. T., Ofek E. O., 2018, *PASP*, **130**, 075002
 Turin G., 1960, *IRE Transactions on Information Theory*, **6**, 311
 Wang S.-Y., et al., 2016, in *Ground-based and Airborne Instrumentation for Astronomy VI*, p. 990846, doi:10.1117/12.2232062
 Waxman E., Bahcall J., 1997, *Physical Review Letters*, **78**, 2292
 West A. A., Weisenburger K. L., Irwin J., Berta-Thompson Z. K., Charbonneau D., Dittmann J., Pineda J. S., 2015, *The Astrophysical Journal*, **812**, 3
 Zhang Z. W., et al., 2013, *AJ*, **146**, 14

ACKNOWLEDGEMENTS

E.O.O. is grateful for the support by grants from the Israel Science Foundation, Minerva, Israeli Ministry of Science, Weizmann-UK, the US-Israel Binational Science Foundation, and the I-CORE Program of the Planning and Budgeting Committee.

Table 1. Observation log

Run start time (UTC)	RA (Deg)	Dec (Deg)	Duration (hours)	Altitude (degrees)	Airmass	Number of objects	Number of flares	In Earth's shadow
06-Aug-2020 18:23:49	272.17	-20.41	0.6	39	1.59	0	0.0	No
06-Aug-2020 19:02:54	305.50	-17.47	2.0	40	1.55	2	81.0	No
06-Aug-2020 21:16:34	334.30	-10.49	2.0	48	1.35	2	45.0	No
06-Aug-2020 23:32:25	10.45	+5.96	2.0	63	1.12	0	0.0	No
07-Aug-2020 01:47:40	58.00	+22.00	1.0	59	1.16	0	0.0	No
07-Aug-2020 20:24:09	331.00	-10.49	1.0	42	1.49	0	0.0	No
08-Aug-2020 21:01:43	331.00	-10.50	0.3	44	1.43	0	0.0	No
10-Aug-2020 19:30:37	272.17	-20.41	0.1	37	1.67	0	0.0	No
10-Aug-2020 19:55:51	272.16	-20.42	1.1	32	1.90	2	14.0	No
10-Aug-2020 21:06:47	272.16	-20.42	0.0	27	2.22	0	0.0	No
10-Aug-2020 17:54:39	305.50	-17.50	0.9	31	1.93	1	7.0	No
10-Aug-2020 21:13:56	337.74	-10.49	2.0	48	1.35	0	0.0	No
10-Aug-2020 23:40:42	331.00	-10.50	0.0	45	1.41	0	0.0	No
10-Aug-2020 23:56:06	331.09	-10.63	2.0	35	1.73	0	0.0	No
11-Aug-2020 02:14:20	98.47	+21.49	0.6	31	1.94	0	0.0	No
11-Aug-2020 19:49:54	305.62	-17.49	0.4	41	1.52	0	0.0	No
11-Aug-2020 17:40:57	275.00	-25.00	0.6	34	1.80	0	0.0	No
11-Aug-2020 19:22:53	305.49	-17.50	0.4	40	1.57	0	0.0	No
12-Aug-2020 18:52:41	272.17	-20.41	0.1	38	1.61	0	0.0	No
12-Aug-2020 19:05:14	272.30	-20.40	0.9	36	1.68	3	25.0	No
12-Aug-2020 17:50:36	305.49	-17.52	0.9	32	1.91	0	0.0	No
13-Aug-2020 20:41:23	331.02	-10.49	0.6	45	1.41	0	0.0	No
13-Aug-2020 21:17:35	331.04	-10.49	1.3	49	1.33	2	44.0	No
13-Aug-2020 22:48:47	10.50	+6.01	1.3	59	1.17	0	0.0	No
14-Aug-2020 00:20:44	330.99	-10.54	1.4	32	1.88	0	0.0	No
14-Aug-2020 02:19:57	10.51	+6.00	0.5	55	1.21	0	0.0	No
14-Aug-2020 17:23:29	272.17	-20.40	1.2	39	1.59	5	48.0	No
14-Aug-2020 18:52:22	272.15	-20.42	2.0	34	1.79	9	34.0	No
14-Aug-2020 21:01:21	331.03	-10.49	1.5	49	1.33	3	75.0	No
14-Aug-2020 22:46:49	10.50	+6.01	1.3	59	1.17	0	0.0	No
15-Aug-2020 00:15:42	29.00	+17.02	2.0	73	1.05	1	3.0	No
15-Aug-2020 02:33:11	29.00	+17.00	0.2	74	1.04	0	0.0	No
15-Aug-2020 17:15:41	272.17	-20.39	1.3	39	1.59	6	53.0	No
15-Aug-2020 18:44:27	272.15	-20.43	2.0	34	1.77	1	2.0	No
15-Aug-2020 21:05:47	331.01	-10.48	1.4	49	1.33	0	0.0	No
15-Aug-2020 22:35:17	10.50	+6.01	1.4	58	1.17	0	0.0	No
16-Aug-2020 00:20:16	29.41	+17.02	2.0	74	1.04	0	0.0	No
16-Aug-2020 02:35:23	29.00	+17.00	0.3	73	1.05	0	0.0	No
16-Aug-2020 18:43:36	272.15	-20.43	2.0	34	1.79	3	8.0	No
16-Aug-2020 17:40:56	305.52	-17.50	0.9	32	1.86	7	24.0	No
16-Aug-2020 21:03:52	331.01	-10.48	1.3	49	1.33	1	2.0	No
17-Aug-2020 18:54:56	272.18	-20.42	2.0	32	1.86	3	10.0	No
17-Aug-2020 17:25:52	305.50	-17.49	1.4	33	1.84	2	12.0	No
17-Aug-2020 21:09:10	305.50	-17.50	1.1	37	1.64	0	0.0	No
17-Aug-2020 22:38:35	10.40	+5.91	1.3	59	1.16	0	0.0	No
18-Aug-2020 00:06:24	29.00	+17.02	2.0	73	1.04	0	0.0	No
18-Aug-2020 02:23:14	29.00	+17.00	0.5	72	1.05	0	0.0	No
18-Aug-2020 19:10:12	272.15	-20.41	1.3	33	1.86	0	0.0	No
19-Aug-2020 18:47:56	272.15	-20.43	1.9	32	1.86	0	0.0	No
20-Aug-2020 00:07:49	29.00	+17.02	1.9	74	1.04	0	0.0	No
20-Aug-2020 02:36:21	58.00	+22.00	0.3	75	1.03	0	0.0	No
20-Aug-2020 18:39:54	272.15	-20.43	2.0	33	1.85	0	0.0	No
20-Aug-2020 17:37:14	305.50	-17.49	0.9	34	1.79	5	56.0	No
20-Aug-2020 20:52:37	342.07	-10.51	2.0	48	1.35	0	0.0	No
20-Aug-2020 23:06:26	10.50	+6.01	0.6	62	1.14	1	2.0	No
20-Aug-2020 23:50:13	29.01	+17.02	2.0	73	1.05	0	0.0	No
21-Aug-2020 02:08:17	29.00	+17.00	0.7	72	1.05	0	0.0	No

Table 1 (cont'd)

Run start time (UTC)	RA (Deg)	Dec (Deg)	Duration (hours)	Altitude (degrees)	Airmass	Number of objects	Number of flares	In Earth's shadow
21-Aug-2020 17:20:07	305.50	-17.49	2.0	36	1.69	0	0.0	No
21-Aug-2020 19:33:50	331.00	-10.49	1.4	44	1.44	0	0.0	Yes
22-Aug-2020 18:02:14	272.16	-20.42	1.5	37	1.67	2	79.0	No
22-Aug-2020 21:16:17	10.50	+6.02	2.0	53	1.26	2	17.0	No
22-Aug-2020 23:28:09	29.01	+17.00	0.1	60	1.16	0	0.0	No
22-Aug-2020 23:41:40	29.00	+17.02	2.0	73	1.05	0	0.0	No
23-Aug-2020 18:09:26	272.16	-20.42	0.9	37	1.65	0	0.0	No
23-Aug-2020 19:10:58	331.00	-10.48	2.0	44	1.43	0	0.0	Yes
23-Aug-2020 21:24:35	10.51	+6.03	2.0	55	1.22	0	0.0	No
23-Aug-2020 23:37:13	28.81	+16.83	2.0	72	1.05	0	0.0	No
24-Aug-2020 01:54:04	29.00	+16.99	1.1	71	1.06	0	0.0	No
24-Aug-2020 20:43:26	10.50	+6.04	2.0	48	1.34	0	0.0	No
24-Aug-2020 23:11:56	10.50	+6.01	0.2	63	1.12	1	6.0	No
25-Aug-2020 00:01:34	29.01	+17.01	0.1	68	1.08	0	0.0	No
25-Aug-2020 00:27:22	29.05	+17.01	1.3	76	1.03	0	0.0	No
25-Aug-2020 01:58:55	29.06	+16.99	1.0	70	1.07	0	0.0	No
25-Aug-2020 17:14:22	294.35	+38.96	2.0	77	1.02	0	0.0	No
25-Aug-2020 19:33:50	331.00	-10.48	2.0	47	1.37	0	0.0	Yes
25-Aug-2020 21:44:56	331.00	-10.50	1.6	46	1.39	0	0.0	Yes
26-Aug-2020 17:13:05	294.36	+38.95	1.9	78	1.02	1	2.0	No
26-Aug-2020 20:27:42	331.01	-10.48	1.2	49	1.33	0	0.0	Yes
26-Aug-2020 21:57:25	10.51	+6.01	1.4	59	1.17	2	80.0	No
26-Aug-2020 23:42:22	30.73	+16.82	2.0	74	1.04	0	0.0	No
27-Aug-2020 01:58:44	29.00	+16.99	1.0	68	1.08	0	0.0	No
27-Aug-2020 19:51:46	294.34	+38.93	1.9	65	1.11	0	0.0	No
27-Aug-2020 18:26:18	331.00	-10.49	1.2	37	1.65	0	0.0	No
27-Aug-2020 21:55:35	10.50	+6.01	1.0	57	1.19	1	17.0	No
28-Aug-2020 17:15:05	294.36	+38.95	1.2	76	1.03	0	0.0	No
28-Aug-2020 19:49:58	294.36	+38.94	0.6	72	1.05	0	0.0	No
28-Aug-2020 18:48:28	333.50	+51.51	0.9	58	1.17	0	0.0	No
29-Aug-2020 17:06:25	294.35	+38.95	1.3	75	1.03	0	0.0	No
29-Aug-2020 21:01:47	294.36	+38.94	1.0	55	1.22	0	0.0	No
29-Aug-2020 22:04:05	10.31	+5.92	2.0	63	1.12	2	45.0	No
10-Sep-2020 17:05:36	272.16	-20.42	1.2	36	1.69	1	10.0	No
10-Sep-2020 19:20:46	331.00	-10.50	0.2	47	1.37	0	0.0	No
14-Sep-2020 18:05:49	272.16	-20.42	0.9	29	2.07	1	12.0	No
14-Sep-2020 16:48:16	305.50	-17.49	1.2	40	1.57	0	0.0	No
15-Sep-2020 16:49:07	272.17	-20.41	1.2	36	1.70	0	0.0	No
17-Sep-2020 19:06:27	305.50	-17.50	0.6	39	1.58	0	0.0	No
18-Sep-2020 16:25:21	272.16	-20.43	1.6	36	1.71	4	18.0	No

Note. — The coordinates are for the centre of the field for that run (in J2000). Also specified is the run duration. The airmass and altitude are taken for the middle of the run. Number of objects is the number of distinct objects, possibly with multiple flares, seen in that run. Number of flares refers to the total number of separate flares from all objects in that run. We define a field to be ‘in Earth’s shadow’ if the line of sight of the centre of the field is inside Earth’s shadow when crossing the height of geosynchronous satellites (~ 37000 km). Such fields are not expected to have any contributions from any satellites up to (and including) geosynchronous orbit.

This paper has been typeset from a \LaTeX file prepared by the author.